

# Eccentric disc instability in stellar discs formed from inspiralling gas clouds in the Galactic Centre

Alessia Gualandris<sup>1,2\*</sup>, Michela Mapelli<sup>3</sup> and Hagai B. Perets<sup>4,5</sup>

<sup>1</sup>*Max-Planck Institut für Astrophysik, Karl-Schwarzschild-Str. 1, D-85741 Garching, Germany*

<sup>2</sup>*Department of Physics and Astronomy, University of Leicester, Leicester, LE1 7RH, United Kingdom*

<sup>3</sup>*INAF-Osservatorio Astronomico di Padova, Vicolo dell'Osservatorio 5, I-35122, Padova, Italy*

<sup>4</sup>*Harvard-Smithsonian Center for Astrophysics, 60 Garden St., Cambridge, MA, USA*

<sup>5</sup>*Technion - Israel Institute of Science, Haifa, Israel 32000*

## ABSTRACT

The inspiral of a turbulent molecular cloud in the Galactic centre may result in the formation of a small, dense and moderately eccentric gas disc around the supermassive black hole (SMBH). Such a disc is unstable to fragmentation and may lead to the formation of young massive stars in the central parsec of the Galaxy. Here we perform high-accuracy direct summation  $N$ -body simulations of a ring of massive stars (with initial semi-major axes  $0.1 \leq a/\text{pc} \leq 0.4$  and eccentricities  $0.2 \leq e \leq 0.4$ ), subject to the potential of the SMBH, a stellar cusp, and the parent gas disc, to study how the orbital elements of the ring evolve in time. The initial conditions for the stellar ring are drawn from the results of previous simulations of molecular cloud infall and disruption in the SMBH potential. While semi-major axes do not evolve significantly, the distribution of eccentricities spreads out very fast ( $\approx 1$  Myr) as a consequence of cusp precession. In particular, stellar orbits with initial eccentricity  $e > 0.3$  ( $e < 0.3$ ) tend to become even more (less) eccentric, resulting in a bimodal eccentricity distribution. The distribution is qualitatively consistent with that of the massive stars observed in the Galactic centre's clockwise disc.

**Key words:** black hole physics – methods: N-body simulations – stars: kinematics and dynamics – Galaxy: centre

## 1 INTRODUCTION

Despite the strong tidal field exerted by the supermassive black hole (SMBH) in the Galactic centre (GC, Morris 1993), more than a hundred young massive stars are observed in the central parsec of the Galaxy.

The majority are O-type and Wolf-Rayet (WR) stars, of which about two thirds show clockwise motion when projected on the plane of the sky while the remainder show counterclockwise motion (Paumard et al. 2006; Nayakshin et al. 2006; Martins et al. 2007; Lu et al. 2009; Bartko et al. 2009). The WR/O stars in the larger group orbit the SMBH in a thin disc, usually referred to as the clockwise (CW) disc, with an estimated age of  $\sim 6$  Myr and an average eccentricity of  $\sim 0.4$ . The smaller group of stars on counter-rotating orbits may indicate the presence of an additional dissolving disc (Bartko et al. 2009; Löckmann & Baumgardt 2009). The CW disc shows a sharp inner truncation at about one arcsecond (or 0.04 pc).

The S-cluster (Schödel et al. 2003; Ghez et al. 2003, 2005; Eisenhauer et al. 2005; Gillessen et al. 2009) located in the innermost arcsecond is a group of about 20 B-type stars moving on eccentric and randomly oriented orbits, with estimated ages of 20 – 100 Myr. The origin of the S-cluster is largely controversial, with main models including the inspiral of a young star cluster (Gerhard 2001; Kim & Morris 2003; McMillan & Portegies Zwart 2003; Gürkan & Rasio 2005; Levin et al. 2005; Fujii et al. 2008), possibly hosting an intermediate-mass black hole (Hansen & Milosavljević 2003; Berukoff & Hansen 2006; Merritt et al. 2009; Gualandris & Merritt 2009; Gualandris et al. 2010; Fujii et al. 2009) and the tidal disruption of binaries on low-angular momentum orbits (Gould & Quillen 2003; Perets et al. 2007; Perets 2009; Perets et al. 2009; Antonini et al. 2010; Perets & Gualandris 2010).

The formation of the CW disc, which represents the target of this work, is also debated, but is often attributed to in-situ star formation from an infalling gas cloud (Morris 1993; Nayakshin & Cuadra 2005; Bonnell & Rice 2008; Mapelli et al. 2008; Wardle & Yusef-Zadeh 2008;

\* E-mail: alessia@mpa-garching.mpg.de

Hobbs & Nayakshin 2009; Alig et al. 2011; Mapelli et al. 2012). In particular, Mapelli et al. (2012), hereafter M12, perform  $N$ -body/Smooth Particle Hydrodynamics (SPH) simulations of the infall of a turbulent molecular cloud toward the GC and study the formation of stars in the region. They find that the tidal disruption of the cloud results in the formation of a small (radius  $< 0.5$  pc), dense ( $> 10^8$  atoms  $\text{cm}^{-3}$ ) and eccentric ( $e \sim 0 - 0.6$ ) gas disc around the SMBH. The simulations by M12 are the first following the fragmentation of the gas disc into self-bound clumps. Stars originate from such clumps in a ring at a distance of  $0.1 - 0.4$  pc with moderately eccentric orbits ( $e \sim 0.2 - 0.4$ ). The mass function of the stars is top-heavy if the local background temperature is sufficiently high ( $\geq 100$  K) and if the parent cloud is sufficiently massive ( $\geq 10^5 M_\odot$ ). These properties are in good agreement with observations of the CW disc (Paumard et al. 2006; Bartko et al. 2009), and lend further support to the in-situ formation model for the disc. The simulations by M12, however, follow the evolution of the system for only about  $0.5$  Myr since the formation of the gaseous disc, whereas the estimated age of the CW disc is of about  $6$  Myr.

Here we use high-accuracy direct summation  $N$ -body simulations to follow the evolution of the stellar ring for  $10$  Myr under the effect of the combined gravitational potential due to the SMBH, the stellar cusp, and the residual gas disc. We stress that this is the first calculation ever performed to follow both the short term star formation phase and the long term evolution of the disc in a consistent manner. We find that the disc retains its initial inner and outer radius, and that stars remain largely confined to the initial ring plane, which is aligned with the gas disc. Interestingly, we observe evidence of the eccentric disc instability described by Madigan et al. (2009), according to which precession of the orbits due to the presence of the stellar cusp induces coherent torques that drive orbital eccentricities away from their initial values. As a result, a bimodal eccentricity distribution is established which is consistent with observations of the CW disc in the GC (Bartko et al. 2009).

## 2 N-BODY SIMULATIONS

We use the direct summation  $N$ -body code  $\phi$ GRAPE (Harfst et al. 2007) modified to include the effects of an external potential due to the stellar cusp and the gas disc. We adopt a mass of  $M_\bullet = 3.5 \times 10^6 M_\odot$  for the SMBH and the broken power-law profile of Genzel et al. (2003) for the stellar cusp density

$$\rho(r) = \rho_0(r_0/r)^\gamma \quad (1)$$

with  $r_0 = 10'' \sim 0.39$  pc,  $\rho_0 = 1.2 \times 10^6 M_\odot \text{pc}^{-3}$ ,  $\gamma = 1.4$  for  $r < r_0$  and  $\gamma = 2.0$  for  $r \geq r_0$ . For the residual gas disc we adopt a projected density profile of the type

$$\Sigma(R) = \Sigma_0(R_0/R)^\alpha \quad (2)$$

with parameters  $\alpha = 1.14$ ,  $R_0 = 1$  pc and  $\Sigma_0 = 2.64 \times 10^3 M_\odot \text{pc}^{-2}$  derived from fitting a power-law profile to the gas remaining after star formation in the simulation of M12. The mass profile of the stellar cusp and gas disc are shown in Fig. 1. The gravitational potential generated by a thin disc

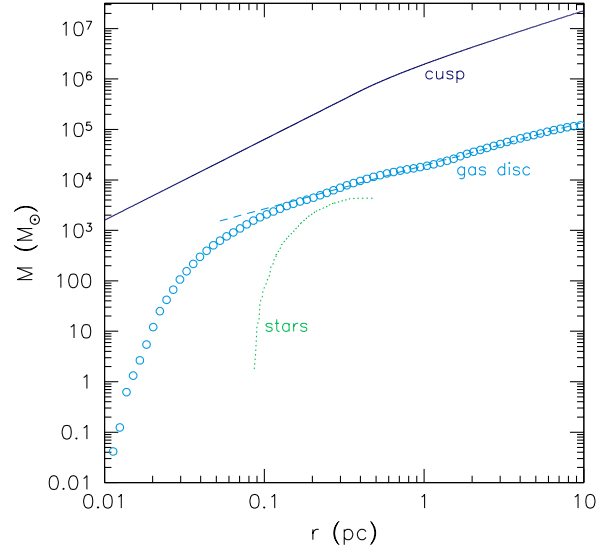


**Figure 1.** Solid line: mass profile of the stellar cusp whose gravitational effect is included in the simulations in the form of an analytic external potential. Points: mass profile of the gaseous disc obtained by the SPH simulations of M12. Dashed line: power-law fit to the gas disc profile adopted to generate the external potential by means of Eq. 3. Dotted line: mass profile of stellar ring as obtained by M12 and used as initial conditions for the integrations.

of known  $\Sigma(R)$  is given by the integral (Binney & Tremaine 1987, Eq.2-142b)

$$\Phi(R, z) = -\frac{2G}{\sqrt{R}} \int_0^\infty \mathcal{K}(k) k \Sigma(R') \sqrt{R'} dR' \quad (3)$$

where

$$k = \sqrt{\frac{4RR'}{(R+R')^2 + z^2}} \quad (4)$$

and  $\mathcal{K}(k)$  represents the complete elliptic integral of the first kind. Differentiating Eq. 3 with respect to  $R$  and  $z$  gives

$$\begin{aligned} \frac{\partial \Phi}{\partial R}(R, z) &= \frac{G}{R^{3/2}} \int_0^\infty \left[ \mathcal{K}(k) - \frac{1}{4} \left( \frac{k^2}{1-k^2} \right) \mathcal{E}(k) \right. \\ &\quad \left. \times \left( \frac{R'}{R} - \frac{R}{R'} + \frac{z^2}{RR'} \right) \right] k \Sigma(R') \sqrt{R'} dR' \quad (5) \end{aligned}$$

and

$$\frac{\partial \Phi}{\partial z}(R, z) = 4Gz \int_0^\infty \frac{\mathcal{E}(k)}{1-k^2} \frac{\Sigma(R') R' dR'}{[(R+R')^2 + z^2]^{3/2}}, \quad (6)$$

where  $\mathcal{E}(k)$  represents the complete elliptic integral of the second kind. The equations for the gravitational potential and forces can be solved numerically on a cylindrical coordinate grid.

Relevant timescales for the stars are shown in Fig. 2 as a function of distance from the SMBH. At distances of  $0.1 - 0.4$  pc, precession due to general relativity (GR) is not important on timescales of  $10$  Myr, and we therefore neglect it in the simulations. On the other hand, Newtonian precession due to the stellar mass distributed within the orbits of

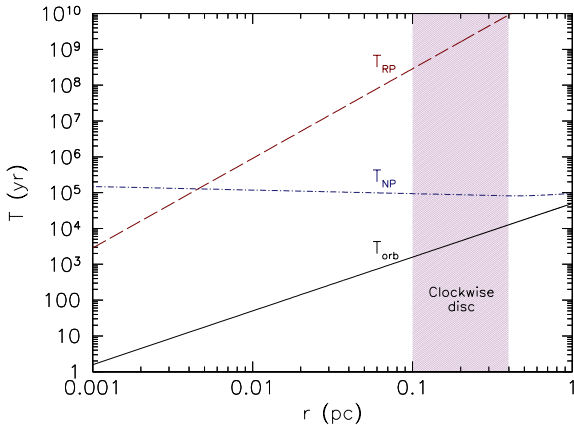


**Figure 2.** Relevant timescales for the ring stars in the GC: orbital period (solid line), timescale of GR precession (dashed lines) and timescale for Newtonian precession (dot-dashed line). The shaded area indicates the approximate location of the CW disc. An orbital eccentricity of 0.3 is assumed.

the stars has a timescale of (e.g. Merritt et al. 2011)

$$T_{\text{NP}} = \frac{M_{\bullet}}{M_{\text{cusp}}} T_{\text{orb}} f(e), \quad (7)$$

where  $T_{\text{orb}}$  is the orbital period of a star with semi-major axis  $a$ ,  $M_{\text{cusp}}$  is the total stellar mass enclosed within the orbit and

$$f(e) = \frac{1 + \sqrt{1 - e^2}}{\sqrt{1 - e^2}}.$$

$T_{\text{NP}}$  is of about  $10^5$  yr for the stars in the ring. For  $\gamma = 3/2$ ,  $T_{\text{NP}}$  is independent of  $a$ . For our adopted broken power-law profile,  $T_{\text{NP}}$  is only weakly dependent on distance (see Fig. 2).

## 2.1 Initial conditions

We adopt the outcomes of run E by M12 as initial conditions for the simulations presented in this paper. In particular, M12 performed N-body/SPH simulations of a gas cloud evolving in the potential of a  $M_{\bullet} = 3.5 \times 10^6 M_{\odot}$  SMBH and a stellar cusp as described in Eq. 1. The impact parameter of the cloud with respect to the SMBH is  $10^{-2}$  pc and the initial velocity is close to the escape velocity from the SMBH at the initial distance (25 pc). The cloud is quite massive ( $1.3 \times 10^5 M_{\odot}$ ), initially spherical (with a radius of 15 pc), marginally self-bound and seeded with supersonic turbulent velocities. The thermodynamic treatment in run E includes radiative cooling with accurate recipes for opacity (Boley 2009) and an irradiation temperature  $T_{\text{irr}} = 100$  K, mimicking the background temperature of the GC. Due to the SMBH shear, the molecular cloud is disrupted in  $\approx 10^5$  yr and, because of its low orbital angular momentum, part of the gas settles in a very small and dense disc surrounding the SMBH (see Fig. 3). A fraction of the gas in the disc fragments forming self-bound clumps (with density  $\geq 2 \times 10^{12} \text{ cm}^{-3}$ ). As a combined effect of the initial cloud mass and of the floor temperature, the mass function of the clumps is top-heavy, ranging between 1 and  $60 M_{\odot}$  after  $4.8 \times 10^5$  yr.

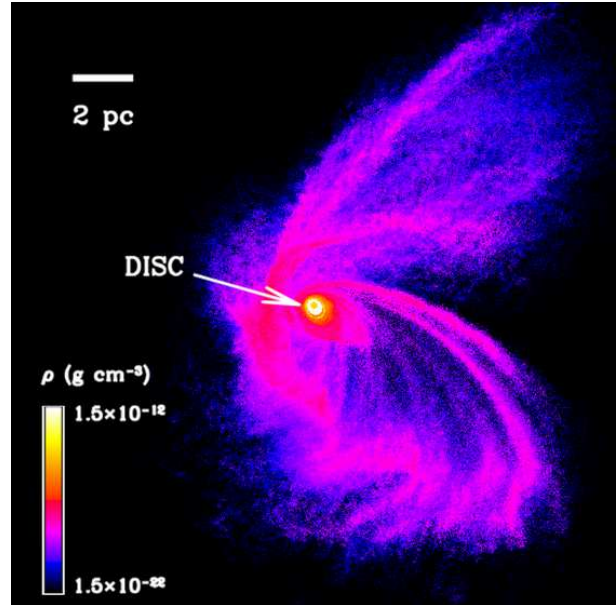


**Figure 3.** Density map of the gas in run E of M12 at  $t = 4.8 \times 10^5$  yr. The simulation was projected in the plane where the gaseous disc (at the centre) is seen face-on. The box measures 20 pc per edge.

Here we assume that each self-bound clump formed in run E of M12 becomes a star, without accreting any further gas particles after  $t = 4.8 \times 10^5 \text{ yr}^1$ . Thus, we replace each gas clump with a single star particle having mass equal to the total mass of the clump itself, and position and velocity corresponding to those of the centre-of-mass of the clump. The resulting stellar ring, with a total mass of  $\sim 4.3 \times 10^3 M_{\odot}$ , is shown in the top panels of Fig. 4. The edge-on view shows a small degree of warping.

In this paper, we cannot integrate the star particles together with the gas particles, as it would be prohibitive to follow the gas for  $\gtrsim 1$  Myr. Thus, we substitute the remaining gas particles with an analytical potential (Eq. 2) very close to the final distribution of gas in run E of M12 (see their figure 10). The total mass of the gas disc within 0.4 pc (i.e. the outer edge of the stellar ring) is  $\sim 10^4 M_{\odot}$ . For simplicity, the potential is assumed constant in time. While this assumption may seem unrealistic, it is justified by the fact that the evolution of the ring stars is dominated by the SMBH and the stellar cusp, and the gas disc potential represents a small correction to the total potential. We performed an additional simulation excluding the gas disc potential and we found a very similar evolution for the ring stars.

The SMBH is treated as a point-mass  $N$ -body particle, similarly to the ring stars. However, given the small number of particles in the simulations, the SMBH would be subject to an unrealistically large motion at the center of the potential well (Merritt 2005), which might affect the dynamics of the stars. For this reason, at each integration step we force the SMBH to remain fixed at the center of the reference frame.

<sup>1</sup> This assumption is quite conservative for the masses of stars, as it is realistic to expect further gas accretion in run E of M12.

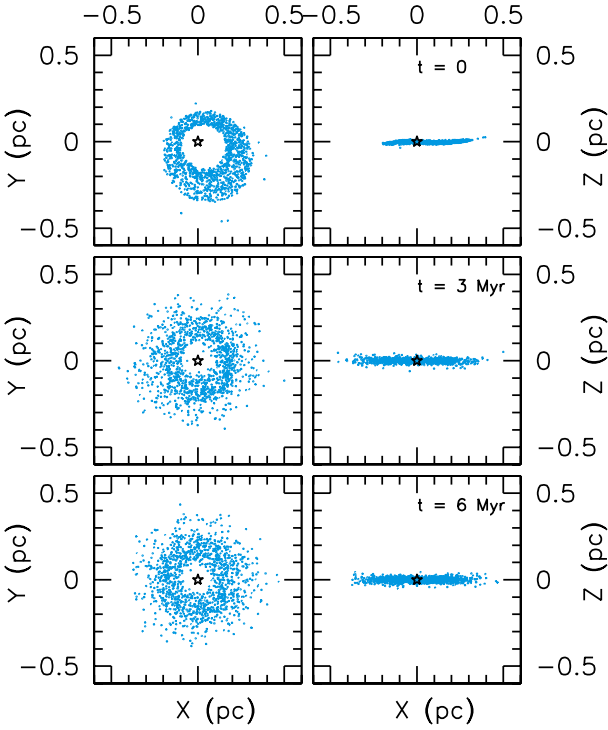


**Figure 4.** Snapshots of the ring stars at different times during the evolution (from top to bottom  $t = 0, 3, 6$  Myr, in a reference frame in which the stars lie in the  $x - y$  plane. The star symbol marks the position of the SMBH.

### 3 RESULTS

We let the ring of stars evolve for 10 Myr under the effect of the gravitational potential generated by the SMBH, the stellar cusp, and the gas disc. Due to the presence of extended mass (stars and gas) within the orbit of each ring star, stars precess in their orbital plane. Because of its much higher mass, the stellar cusp is responsible for most of the precession. While the dependence of the precession time on distance is rather weak (see Fig. 2), the dependence on eccentricity may be significant. This implies a different precession time for stars with different eccentricity, and it results in a quick loss of coherence in the ring, as can be seen from the snapshots at 3 Myr and 6 Myr shown in Fig. 4. Only in the absence of a stellar cusp would the ring evolve coherently.

The orbital elements of all stars are shown in Fig. 5, at different times during the integration. While the semi-major axes distribution remains unchanged during the evolution, the distribution of eccentricities evolves toward a bimodal distribution, as can be seen in Fig. 6. While the initial distribution of eccentricities shows a single peak at  $e \sim 0.3$ , the distribution after 6 Myr has a primary peak at  $e \sim 0.1$  and a secondary peak at  $e \sim 0.5$ , with a tail that extends to about  $e \sim 0.7$ . The cumulative distributions of eccentricities are shown in the insert.

We attribute this behaviour to the eccentric disc instability which was predicted to occur in eccentric discs subject to cusp precession (Madigan et al. 2009). Due to the fact that  $f(e)$  in Eq. 7 is a monotonically increasing function of eccentricity, an orbit with initial eccentricity in excess of the average will have a longer precession time, which will

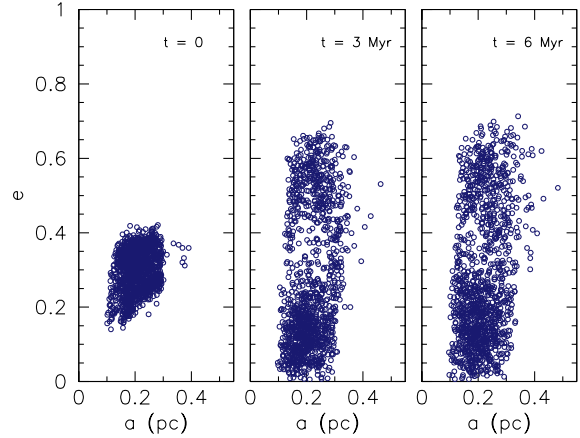


**Figure 5.** Orbital elements of the ring stars at the start of the integration (left panel), after 3 Myr (middle panel) and after 6 Myr of evolution (right panel).

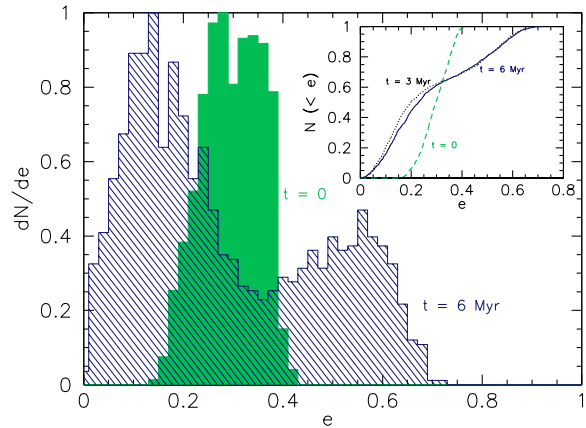


**Figure 6.** Eccentricity distribution of the ring stars at the start of the integration (filled area) and after 6 Myr of evolution (hatched area). The insert in the top-right corner shows the cumulative distribution of eccentricities at different times: at the beginning of the integration (dashed line), after 3 Myr (dotted line) and after 6 Myr (solid line).

result in a stronger torque from the other stars in the ring. The torque will reduce its angular momentum and therefore cause an increase in eccentricity. The opposite effect will happen to stars with orbits initially more circular than the average. The instability is illustrated in Fig. 7, which shows the time evolution of the orbital eccentricity for a random subset of stars in the ring. While stars initially more eccentric than the average ( $\sim 0.3$ ) tend to become more eccentric, stars initially less eccentric than the average tend to circularise. The observed timescale for the process is of only  $\sim 1$  Myr. This is in agreement with the predicted timescale (Madigan et al. 2009)

$$T_{\text{ecc}} \sim T_{\text{NP}} \left( \frac{M_{\text{cusp}}}{M_{\text{ring}}} \right)^{1/2} \left[ e \sqrt{1 - e^2} \frac{d}{de} \left( \frac{1}{f(e)} \right) \right]^{-1/2}, \quad (8)$$

where  $M_{\text{cusp}}$  and  $M_{\text{ring}}$  are the cusp mass and the ring mass, respectively. In our case,  $30 \lesssim M_{\text{cusp}}/M_{\text{ring}} \lesssim 60$  for  $0.1 \lesssim$

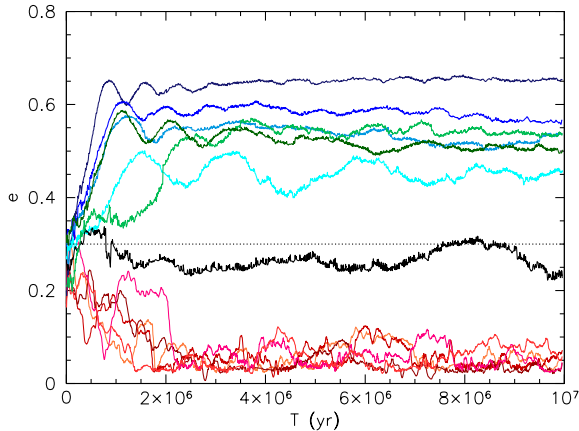


**Figure 7.** Eccentric orbit instability in a random subset of stars. The timescale for the process is about 1 Myr.

$r/\text{pc} \leq 0.4$  and  $T_{\text{ecc}} \sim 5 - 10$  for a circular orbit. As the ring loses coherence after this time, torques become weaker and changes in the eccentricities become less pronounced.

This distribution is consistent with, though not identical to, the one found for the CW disc. Bartko et al. (2009) perform a statistical analysis of the candidate disc members, assuming Keplerian orbits in the gravitational potential of the SMBH and the stellar cusp, and derive distributions for the orbital elements of the stars. While these distributions are subject to many uncertainties, the main properties of the eccentricity distribution appear robust. In particular, they report a bimodal distribution for the reconstructed eccentricities with peaks at  $e \sim 0.3$  and  $0.9$ , though they caution that the high eccentricity stars may not dynamically belong to the disc. Once corrected for projection effects, the mean eccentricity in the CW disc is  $\sim 0.37$ , only slightly higher than what we find. The difference is likely due to the eccentricity with which the stars form from the gas disc, which in turn depends on the orbital parameters of the cloud. An average eccentricity of  $\gtrsim 0.4$  could be produced starting with an even more radial orbit for the molecular cloud, which might result from cloud-cloud collisions near the GC (e.g. Hobbs & Nayakshin 2009). Very large eccentricities ( $\gtrsim 0.99$ ) like those found by Madigan et al. (2009), however, seem hard to produce even starting from a more eccentric gas disc. This has important implications for models of the origin of the S-cluster in the GC. For tidal disruption and capture to occur, a binary must come at least as close to the SMBH as the tidal radius. Madigan et al. (2009) find that for a  $4 \times 10^3 M_{\odot}$  disc with initial eccentricity of  $0.6$  the maximum eccentricity attained by the stars is about  $0.9$ , and yet there are no stars with a pericentre distance small enough to be tidally disrupted. Only discs more massive than  $10^4 M_{\odot}$  and with initial eccentricities in excess of  $0.6$  result in a significant number of tidal disruptions. We conclude that the S-stars cannot have formed from a disc like the one produced here.

In addition to finding smaller eccentricities than in some of Madigan’s simulations, we find smaller inclinations with respect to the initial ring plane. Inclinations after 6 Myr are generally smaller than  $\sim 10$  degrees and the maximum we record is  $\sim 16$  degrees. Inclinations do not seem to correlate

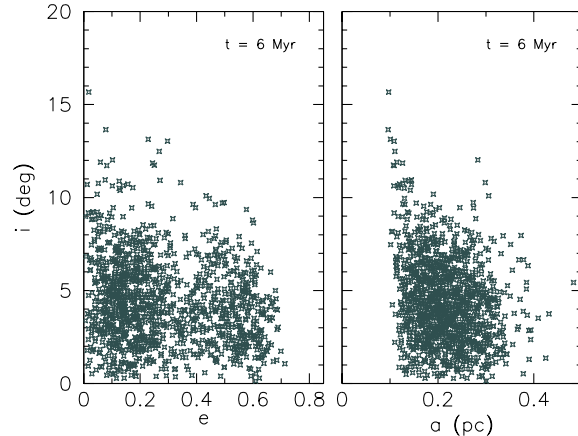


**Figure 8.** Inclinations of the ring stars after 6 Myr of evolution as a function of eccentricity (left panel) and semi-major axis (right panel). The inclination is calculated as the angle between the angular momentum of the star and the z-axis, which is parallel to the initial total angular momentum of the ring.

with eccentricities (see Fig. 8), though we note that if we divide the sample of stars in two groups, having  $e < 0.3$  and  $e \geq 0.3$ , the inclinations in the two groups evolve in a different way. A 2D Kolmogorov-Smirnov test gives probability values of  $0.07$  at the start of the simulation,  $0.01$  after 3 Myr and  $2.1 \times 10^{-6}$  after 6 Myr that the inclinations in the two groups originate from the same distribution. This difference is likely due to differential heating between more eccentric and less eccentric stars. On the other hand, Fig. 8 shows a trend for higher inclinations to develop for stars closer to the SMBH. This is a result of the initial warping present in the stellar ring, which in turn reflects the warping of the gas disc. Larger inclinations might originate from more strongly warped gas discs, but additional SPH simulations would be required to test this scenario. The rms inclination grows slowly with time, roughly as  $t^{1/8}$ , while the rms eccentricity remains approximately constant at  $e \approx 0.3$ . This scaling is somewhat flatter than what is found in Cuadra et al. (2008) and Haas & Šubr (2012), and it may be attributed to the different initial conditions adopted in this work, in particular to the non zero mean initial eccentricity and/or warping of the stellar ring. The modest inclinations achieved by the simulated stars imply that the single cloud infall scenario cannot account for the high inclination of some of the young stars observed in the GC (those claimed to belong to a counterclockwise disc). A cloud-cloud collision has been shown to produce significantly warped stellar discs and additional filamentary structures at large inclinations with respect to the disc (Hobbs & Nayakshin 2009). Alternatively, the interaction between two approximately coeval and highly inclined stellar discs may provide an explanation for the existence of stars at high inclination (Löckmann & Baumgardt 2009).

Finally, we find a very modest heating of the stellar ring during the evolution. This is likely due to the absence of heating from the stellar cusp in our simulations, which would result in an increase in the mean ring height (see e.g. Perets et al. 2008).

#### 4 DISCUSSION AND CONCLUSIONS

We studied the evolution of the ring of stars formed in the GC from fragmentation of the gas disc deposited by an in-spiralling molecular cloud. Our calculation is the first of its kind to follow, in a consistent manner, both the star formation phase in the gaseous disc and the long term evolution of the stellar disc. We find that, while the ring retains the original distribution of semi-major axes, and therefore also the initial inner and outer radius, the distribution of eccentricities evolves in time due to the onset of the eccentric disc instability. Torques exerted by other stars in the ring result in a change in the magnitude of the angular momentum and, as a consequence, in the eccentricity. As stars evolve away from the average eccentricity, a bimodal distribution is established, with a primary peak at  $e \sim 0.1$ , a secondary peak at  $e \sim 0.5$ , and a tail that extends to  $e \sim 0.7$ . This is qualitatively consistent with the distribution found for the CW disc stars. We predict that a quantitative agreement would require a molecular cloud with an initial orbit more radial than in run E of M12, but a new suite of hydrodynamical simulations is necessary to test this prediction. On the other hand, even a better description of the cloud thermodynamics and of the gas shocks taking place during the infall of the cloud might affect the formation and thus the orbital properties of the young stellar ring (see e.g. the discussion in Jiang & Goodman 2011, and references therein).

Our simulations support the scenario in which the thin CW disc originated from fragmentation of a moderately eccentric gas disc resulting from the tidal disruption of a turbulent molecular cloud on a low angular momentum orbit. The origin of the WR/O stars at large inclinations, as well as those belonging to the S-cluster, however, seems to require additional physical processes, which are currently under investigation. In the case of the S-stars, relaxation processes against the background spherical cusp of stars and remnants are unable to explain the observed distribution of eccentricities within the lifetime of the stars (Perets et al. 2009) and different mechanisms are required (for a review see e.g. Perets & Gualandris 2010). Similarly, Cuadra et al. (2008) have shown that relaxation in the disc does not produce eccentricities and inclinations as large as those observed for the WR/O stars outside the CW disc. While some outliers may be the result of vector resonant relaxation between the disc and the stellar cusp (Kocsis & Tremaine 2011), several authors have investigated the possibility of an additional perturbing potential, which would produce Kozai-Lidov type oscillations (Kozai 1962; Lidov 1962) in the eccentricity and inclination of the stars. In particular, Šubr et al. (2009) suggest that precession due to the gravity of the circumnuclear disc (CND) at the edge of the SMBH's sphere of influence might have driven some of the stars away from the CW disc. An axisymmetric perturbation due the presence of an additional gas/stellar disc, an intermediate-mass black hole or the CND might have observable effects also on the stars in the CW disc. Löckmann et al. (2008) studied the effect of a second highly inclined stellar disc, while Šubr et al. (2009) and Haas et al. (2011) considered the effect of the CND. Löckmann et al. (2008) found that, in the absence of a stellar cluster, precession and Kozai oscillations due to the presence of a second, inclined disc result in stars achieving high eccentricities. The inclusion of a stellar cusp, however,

has been shown to damp Kozai oscillations in the disc (e.g. Chang 2009; Löckmann et al. 2009), at least in the case of an analytic spherical cusp. In this case, the overall influence of the cusp can be characterised by a decrease in the amplitude of the eccentricity and inclination oscillations, and by a shortening of their period (Karas & Šubr 2007; Šubr et al. 2009). Chang (2009) examined the effectiveness of the Kozai mechanism induced by stellar discs in the Galactic centre and found that Kozai oscillations are suppressed if the period for apsidal precession induced by the cusp is shorter than the period for Kozai oscillations. In the case of the two disc scenario, the mass of the stellar cusp in the GC is over an order of magnitude larger than the critical mass required to suppress the Kozai mechanism.

In general, the damping of the Kozai mechanism depends on the parameters of the perturbing potential and on the orbital parameters of the stars, and oscillations might be important for certain sets of parameters. The period of Kozai oscillations can be written as (Šubr et al. 2009)

$$T_K = \frac{M_\bullet}{M_P} \frac{R_P^3}{a\sqrt{GM_\bullet a}} \sim \frac{M_\bullet}{M_P} \left(\frac{R_P}{a}\right)^3 T_{\text{orb}} \quad (9)$$

where  $M_P$  and  $R_P$  are the mass and radius of the perturbing axisymmetric potential. If the perturber is a second disc at approximately the same distance as the CW disc from the SMBH,  $R_P \sim a$  and  $T_K/T_{\text{NP}} \approx M_{\text{cusp}}/M_P$ . If the perturber is the CND, then  $R_P \sim (5-20)a$ . In both cases, it seems unlikely that Kozai oscillations might dominate the evolution of the CW disc in the presence of a spherical cusp. The timescale for Kozai oscillations is also typically longer than the timescale for the eccentric disc instability (see Eq. 8), suggesting that Kozai oscillations should not significantly affect the development of the eccentricity growth studied here, even if this is theoretically possible for certain combinations of parameters.

Löckmann et al. (2009) explored the effect of a granular  $N$ -body cusp as opposed to an analytic smooth cusp. They found that both a smooth and a granular cusp consistent with the one derived for the GC (Schödel et al. 2007) suppress Kozai cycles in the two disc scenario. However, in the case of an  $N$ -body cusp, two-body and resonant relaxation effects may temporarily drive the eccentricity of some stars to large values. This effect is a function of the cusp granularity, i.e. of the mean and maximum stellar masses, and is most efficient in the case of a cusp of stellar remnants. Similar results were obtained by Haas & Šubr (2012).

It is not yet clear whether secular evolution can play an important role under realistic conditions, i.e. a realistic gravitational potential and granularity of the stellar cusp. Shape and parameters of the potential of an additional disc and/or the CND are not well determined, and the exact composition of the GC cusp is not well known. Further investigation of these issues is deemed necessary and will be presented in an upcoming work.

#### ACKNOWLEDGMENTS

We thank the referee Ladislav Šubr for useful comments that helped improve the manuscript. The simulations were performed on the GPU enabled machines at the Max-Planck

Institute for Astrophysics in Garching, Germany. MM acknowledges financial support from INAF through grant PRIN-2011-1.

## REFERENCES

- Alig C., Burkert A., Johansson P. H., Schartmann M., 2011, *MNRAS*, 412, 469
- Antonini F., Faber J., Gualandris A., Merritt D., 2010, *ApJ*, 713, 90
- Bartko H. et al., 2009, *ApJ*, 697, 1741
- Berukoff S. J., Hansen B. M. S., 2006, *ApJ*, 650, 901
- Binney J., Tremaine S., 1987, *Galactic dynamics*
- Boley A. C., 2009, *ApJL*, 695, 53
- Bonnell I. A., Rice W. K. M., 2008, *Science*, 321, 1060
- Chang P., 2009, *MNRAS*, 393, 224
- Cuadra J., Armitage P. J., Alexander R. D., 2008, *MNRAS*, 388, L64
- Eisenhauer F. et al., 2005, *ApJ*, 628, 246
- Fujii M., Iwasawa M., Funato Y., Makino J., 2008, *ApJ*, 686, 1082
- Fujii M., Iwasawa M., Funato Y., Makino J., 2009, *ApJ*, 695, 1421
- Genzel R. et al., 2003, *ApJ*, 594, 812
- Gerhard O., 2001, *ApJL*, 546, L39
- Ghez A. M. et al., 2003, *ApJL*, 586, L127
- Ghez A. M., Salim S., Hornstein S. D., Tanner A., Lu J. R., Morris M., Becklin E. E., Duchêne G., 2005, *ApJ*, 620, 744
- Gillessen S., Eisenhauer F., Trippe S., Alexander T., Genzel R., Martins F., Ott T., 2009, *ApJ*, 692, 1075
- Gould A., Quillen A. C., 2003, *ApJ*, 592, 935
- Gualandris A., Gillessen S., Merritt D., 2010, *MNRAS*, 409, 1146
- Gualandris A., Merritt D., 2009, *ApJ*, 705, 361
- Gürkan M. A., Rasio F. A., 2005, *ApJ*, 628, 236
- Haas J., Šubr L., 2012, *Journal of Physics Conference Series*, 372, 012059
- Haas J., Šubr L., Kroupa P., 2011, *MNRAS*, 412, 1905
- Hansen B. M. S., Milosavljević M., 2003, *ApJL*, 593, L77
- Harfst S., Gualandris A., Merritt D., Spurzem R., Portegies Zwart S., Berczik P., 2007, *New Astronomy*, 12, 357
- Hobbs A., Nayakshin S., 2009, *MNRAS*, 394, 191
- Jiang Y.-F., Goodman J., 2011, *ApJ*, 730, 45
- Karas V., Šubr L., 2007, *A&A*, 470, 11
- Kim S. S., Morris M., 2003, *ApJ*, 597, 312
- Kocsis B., Tremaine S., 2011, *MNRAS*, 412, 187
- Kozai Y., 1962, *AJ*, 67, 591
- Levin Y., Wu A., Thommes E., 2005, *ApJ*, 635, 341
- Lidov M. L., 1962, *Planetary Space Sci.*, 9, 719
- Löckmann U., Baumgardt H., 2009, *MNRAS*, 394, 1841
- Löckmann U., Baumgardt H., Kroupa P., 2008, *ApJL*, 683, L151
- Löckmann U., Baumgardt H., Kroupa P., 2009, *MNRAS*, 398, 429
- Lu J. R., et al., 2009, *ApJ*, 690, 1463
- Madigan A.-M., Levin Y., Hopman C., 2009, *ApJL*, 697, L44
- Mapelli M., Hayfield T., Mayer L., Wadsley J., 2008, *ArXiv e-prints*
- Mapelli M., Hayfield T., Mayer L., Wadsley J., 2012, *ApJ*, 749, 168
- Martins F., Genzel R., Hillier D. J., Eisenhauer F., Paumard T., Gillessen S., Ott T., Trippe S., 2007, *A&A*, 468, 233
- McMillan S. L. W., Portegies Zwart S. F., 2003, *ApJ*, 596, 314
- Merritt D., 2005, *ApJ*, 628, 673
- Merritt D., Alexander T., Mikkola S., Will C. M., 2011, *Phys. Rev. D*, 84, 044024
- Merritt D., Gualandris A., Mikkola S., 2009, *ApJL*, 693, L35
- Morris M., 1993, *ApJ*, 408, 496
- Nayakshin S., Cuadra J., 2005, *A&A*, 437, 437
- Nayakshin S., Dehnen W., Cuadra J., Genzel R., 2006, *MNRAS*, 366, 1410
- Paumard T. et al., 2006, *ApJ*, 643, 1011
- Perets H. B., 2009, *ApJ*, 690, 795
- Perets H. B., Gualandris A., 2010, *ApJ*, 719, 220
- Perets H. B., Gualandris A., Kupa G., Merritt D., Alexander T., 2009, *ApJ*, 702, 884
- Perets H. B., Gualandris A., Merritt D., Alexander T., 2008, *Mem. Soc. Astron. Italiana*, 79, 1100
- Perets H. B., Hopman C., Alexander T., 2007, *ApJ*, 656, 709
- Schödel R. et al., 2007, *A&A*, 469, 125
- Schödel R., Ott T., Genzel R., Eckart A., Mouawad N., Alexander T., 2003, *ApJ*, 596, 1015
- Šubr L., Schovancová J., Kroupa P., 2009, *A&A*, 496, 695
- Wardle M., Yusef-Zadeh F., 2008, *ApJL*, 683, 37